ORNL/TM-2021/2215

Kinetics of Hydrogen Desorption from Yttrium Hydride: The Development of Material Characterization Methods

Takaaki Koyanagi
Hanns Gietl
Ben Garrison

M3TC-21OR0403044

September 2021

Approved for public release.
Distribution is unlimted.

ORNL/TM-2021/2215

Transformational Challenge Reactor Program

KINETICS OF HYDROGEN DESORPTION FROM YTTRIUM HYDRIDE: THE DEVELOPMENT OF MATERIAL CHARACTERIZATION METHODS

Takaaki Koyanagi
Hanns Gietl
Ben Garrison

September 2021

Prepared by
OAK RIDGE NATIONAL LABORATORY
Oak Ridge, TN 37831-6283
managed by
UT-BATTELLE LLC
for the
US DEPARTMENT OF ENERGY
under contract DE-AC05-00OR22725

CONTENTS

LIST OF FIGURES

ABSTRACT

Yttrium hydride possesses attractive neutronic and thermal properties for moderator applications as a high-temperature moderator material in advanced thermal neutron spectrum reactors that require small core volumes. For safe operation of the nuclear reactors, it is critical to understand the kinetics of H desorption from yttrium hydride at elevated temperatures. In previous studies, the H desorption flux as a function of temperature was measured by thermal desorption spectroscopy. To fully understand the H desorption kinetics, the amount of H within the specimen must be locally evaluated, especially if this uniformity strongly affects the thermomechanical properties and irradiation resistance of the bulk material.

This study presents current efforts toward developing quantitative mapping methods for an amount of H with a high spatial resolution. High-throughput nanoindentation mapping was used to indirectly probe local H content based on the chemical composition-dependent indentation hardness and elastic modulus. Raman spectral imaging demonstrated its sensitivity to the presence of YH_2, and the intensity map revealed nonuniform H distributions within pellet specimens. This study found that the nanoindentation mapping and Raman spectral imaging are complementary for understanding local chemistry of the hydride specimens.

1. INTRODUCTION

Metal hydrides are attractive options for neutron moderators in thermal nuclear reactors because the atomic density of H is much greater than that in water and in liquid H itself [1]. Among the hydride systems proposed, yttrium hydride possesses a superior high-temperature capability [1,2] that allows a wide temperature window in the reactor operation design. Currently, yttrium hydride is the leading candidate for a neutron moderator in a microreactor developed under the Transformational Challenge Reactor (TCR) program at Oak Ridge National Laboratory (ORNL) [3]. Understanding the kinetics of H desorption from yttrium hydride at elevated temperatures is critically important for safely operating nuclear reactors with a hydride moderator system. Comprehensive experimental data and a predictive model for the H desorption are required for designing reactors and assessing reactor performance under normal operating environments and off-normal events.

In the previous TCR study [2], the H desorption flux as a function of temperature was measured by thermal desorption spectroscopy. The experiment with three types of yttrium hydrides (H/Y ratios of 1.76, 1.84, and 1.87) at a heating rate of 0.5 K/s up to 1,125 K showed that an onset temperature of the H desorption tended to delay with decreasing H/Y ratio. Currently, it is unclear how H diffuses and dissociates within the specimen during annealing. This information will be a foundation of modeling the H desorption behavior. One challenge in extracting such data is the difficulty of probing local H content within a hydride specimen.

Bulk H content is typically measured by the weight gain of sample before and after hydriding [2], which results in a nominal composition, assuming a uniform microstructure. The other methods for the bulk analysis of H include inert gas fusion, thermal desorption spectroscopy, glow discharge optical emission spectroscopy and mass spectrometry, laser-induced breakdown spectroscopy, secondary ion mass spectrometry, nuclear reaction analysis, and elastic recoil detection analysis [4]. Despite various options for the bulk analysis of H, the local H analysis of bulk specimen at a microscale has been limited. One reason for this is that common electron microscopy techniques (e.g., energy-dispersive x-ray spectroscopy) are not sensitive to H. Additionally, the local analysis of lattice constant by high-energy x-ray diffraction and selected area diffraction in transmission electron microscopy might not be promising because the lattice constant of yttrium hydride is not sensitive to the H/Y atomic ratio [2]. One success of

local H analysis was reported by Gong et al. [5], which demonstrated mapping H content via neutron imaging with an effective spatial resolution of 9.6 μm and a H sensitivity of 9 wppm. The downside of this method is limited accessibility to the neutron source in general. To the best of the authors' knowledge, no other method has been acknowledged as a promising experimental method for probing local hydrogen content in bulk hydrides.

The overarching goal of this study is to develop quantitative evaluation methods for local hydrogen content in bulk hydrides. The nonuniformity could be a key parameter for the performance of the hydride material, as discussed in Section 4. This study specifically focused on demonstrating the semiquantitative analysis of hydrogen content in yttrium hydride at a microscopic scale. Two experimental methods were employed: high-throughput nanoindentation mapping and Raman spectral imaging. Nanoindentation hardness and modulus mapping indirectly determine hydrogen content based on the known correlation between the properties and hydrogen content. The previous study found that Vickers hardness and elastic modulus obtained via resonant ultrasound spectroscopy linearly increased with the increasing H/Y atomic ratio [2]. Therefore, nanoindentation could map hydrogen content via hardness and modulus measurements once the relationship between the properties and hydrogen content are established. Raman spectral imaging also employs a similar indirect approach using the reference specimens. Yttrium hydrides YH_2 and YH_3 are "Raman active" and can be evaluated via Raman spectroscopy. The correlation of the Raman spectrum (e.g., intensity, peak position, full width at half maximum) and known chemical composition enable the local evaluation of hydrogen content via Raman mapping. This study complementarily uses nanoindentation mapping and Raman spectral imaging to reveal nonuniform hydrogen content in yttrium hydride specimens.

2. EXPERIMENT

Crack-free bulk yttrium hydride samples with different H/Y atomic ratios were fabricated through the direct interaction of ultrahigh-purity metallic Y (nominal 99.99%) and H at elevated temperatures. The hydriding process was informed by the well-established thermodynamic property of the Y-H binary system. A fully programmable metal hydriding system with continuous H partial pressure and flow control coordinated with precise temperature control was designed and constructed at ORNL. Details of the processing conditions can be found elsewhere [6]. YH_X pellets (10 mm in diameter, 15 mm tall, approximately 5.4 g) were fabricated with H/Y atomic ratios ranging from 1.00 to 1.92. The H concentration was determined by the weight gain of the samples before and after hydriding. This study used the weight gain data to present the nominal chemical composition of the hydride specimens. The hydride pellets were embedded inside epoxy and machined by using a low-speed diamond saw followed by mechanical polishing for cross-sectional nanoindentation mapping and Raman spectral imaging. The epoxy was dissolved before the experiments.

The NanoBlitz 3D nanoindentation mapping of the specimens at an ambient temperature was performed in a TESCAN MIRA3 scanning electron microscope (SEM) by using a Nanomechanics InForce 1000 Actuator with a diamond Berkovich tip. An applied target load of 7 mN was used, and the indentation spacing was set to 2.5–3.0 μm. The indent spacing was around 10 times the target indentation depth to achieve sufficient precision [7]. The indent speed of the nanoindentation mapping was about 1–3 s per indent. Poisson's ratio of 0.25 was used to calculate nanoindentation hardness and modulus.

Chemical analysis of the hydride specimens was performed via Raman spectral imaging by using a Renishaw inVia confocal Raman microscope. The system has a 532 nm laser, and the laser power at the specimen was 25 mW. The spectra were acquired from 250 to 1,500 cm^{-1}. The step size was fixed to 3 μm along the *x* and *y* directions for the Raman mapping experiment. A 50× long working distance objective lens (numerical aperture of 0.50) was used, which focused the laser at an approximately 1.3 μm diameter on the specimen.

Electron backscatter diffraction (EBSD) analysis used an Oxford Instruments Nordlys detector on the TESCAN SEM operated at 20 kV. EBSD data were acquired by using an Oxford Symmetry EBSD detector and Oxford Aztec 3.1 software. Postprocessing analysis used Aztec, the Oxford Tango software. The EBSD orientation map shows grains colored according to the crystallographic surface normal vector.

3. RESULTS

A total of 6,400 indents in a 200 × 200 μm area were generated on the $YH_{1.70}$ sample by the high-throughput nanoindentation mapping. The indentation area grid was observed by SEM, as shown in Figure 1. The map area contains a secondary phase with brighter contrast, which is likely residual Y detected by x-ray diffraction [2]. The Y phase could contain a certain amount of H because H has 21 at % solubility in Y at ambient temperature [8]. Several indents were observed on the secondary phase, so the indentation spacing of 2.5 μm was sufficiently narrow to evaluate different phases in the specimen.

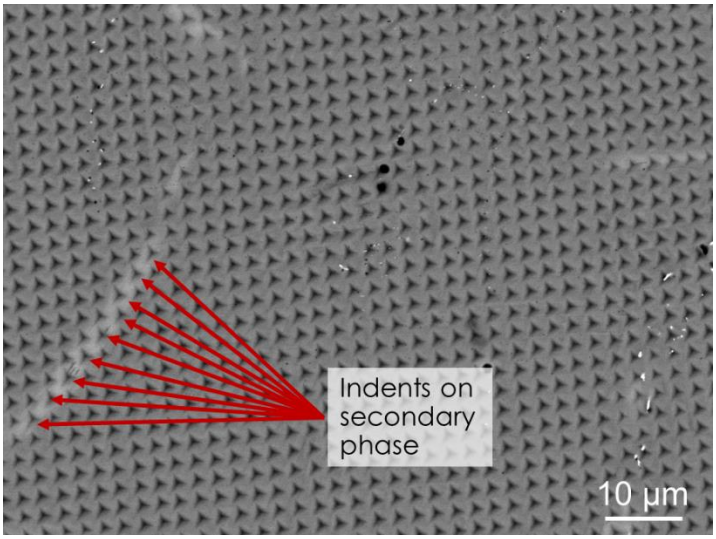

Figure 1. Backscattered electron image of indentation grid on the $YH_{1.70}$ specimen.

Figure 2a shows the nanoindentation modulus map of the $YH_{1.70}$ specimen. Approximately 90% of the area exhibited the elastic modulus of 130–170 GPa. Importantly, the modulus map indicates phases with a lower modulus (~100 GPa or less), which are indicated by the red arrows in Figure 2a. This was confirmed by an EBSD map that covered the indentation grid (Figure 2b). The orientation map was made by fitting the Kikuchi patterns with a face-centered cubic (FCC) YH_2 structure data (space group 225). Phases at the indents were not identified because of the structural damage and/or uneven surface. Phase could not be identified at the secondary phase (dark regions in Figure 2b) because of the low-quality Kikuchi patterns. Comparing the modulus and EBSD maps shows that the low modulus area corresponds to the unidentified region, which indicates that the nanoindentation map is sensitive to the secondary phase. The effects of crystal orientation on the modulus were not clearly identified.

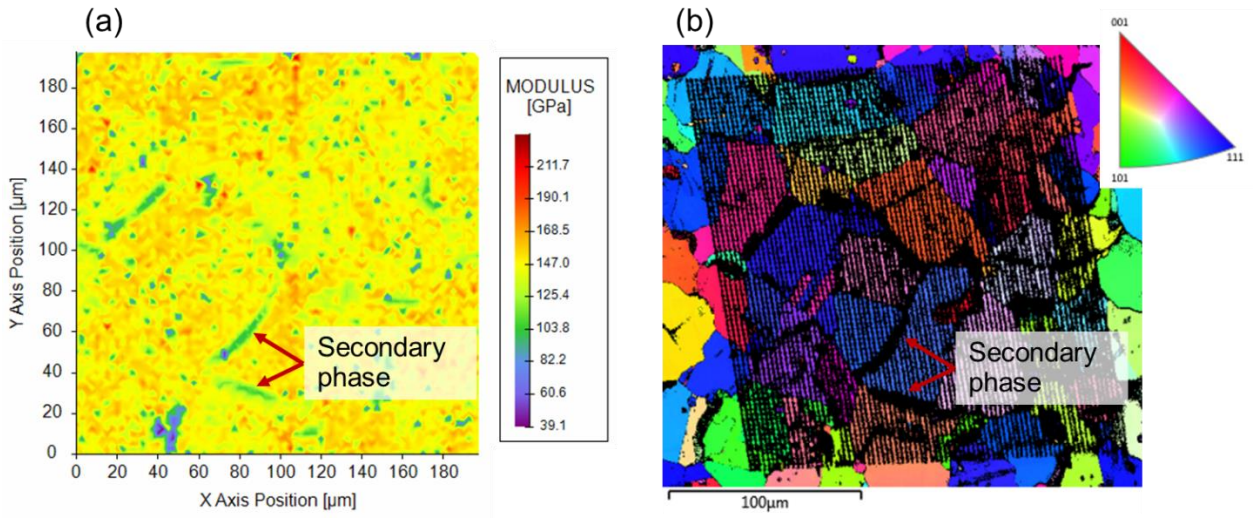

Figure 2. (a) Nanoindentation modulus map and (b) EBSD surface normal-projected inverse pole figure orientation map of the $YH_{1.70}$ specimen.

This study also shows the sensitivity of nanoindentation hardness to H content. Figure 3 shows the hardness map of the $YH_{1.92}$ specimen. The map shows nonuniform hardness ranging from 1 to >10 GPa within a 360 × 360 μm area. The low hardness region indicates the presence of the residual Y, which was found via x-ray diffraction [2]. Figure 3 also shows the inserted Raman intensity map of the YH_2 peak. The baseline-corrected intensity was integrated from 1,055 to 1,225 cm^{-1}. Typical Raman spectra of the region with a hardness of approximately >5GPa in the $YH_{1.92}$ specimen are presented in Figure 4. YH_2 shows a peak at ~1,140 cm^{-1} attributed to the F_{2g} Raman mode of FCC YH_2 [9]. The different intensities of YH_2 peak obtained from the same specimen indicate nonuniform H distribution within the specimen. The Raman spectra also show a peak at ~340 cm^{-1}. The authors tentatively attribute this peak to the CaF_2 peak reported at 322 cm^{-1} because of the impurity CaF_2 precipitates found in the YH_2 grains via transmission electron microscopy [2]. The discrepancy of the peak position could be explained by peak shifts due to lattice strain [10] and small coherent domain size [11].

The direct comparison of the nanoindentation hardness map and the Raman intensity found that the harder area tends to show stronger Raman signal thus more hydride. For example, the left bottom of the Raman map showed very weak YH_2 peak which corresponds to soft area, likely unreacted yttrium. At the middle of the Raman map, strong YH_2 signals are observed, and the area possesses relatively high indentation hardness. The top right of the Raman map shows the lower intensity and lower hardness values. Since the higher H content is expected to exhibit higher hardness [2], the relationship between the hardness and Raman intensity distributions appears reasonable.

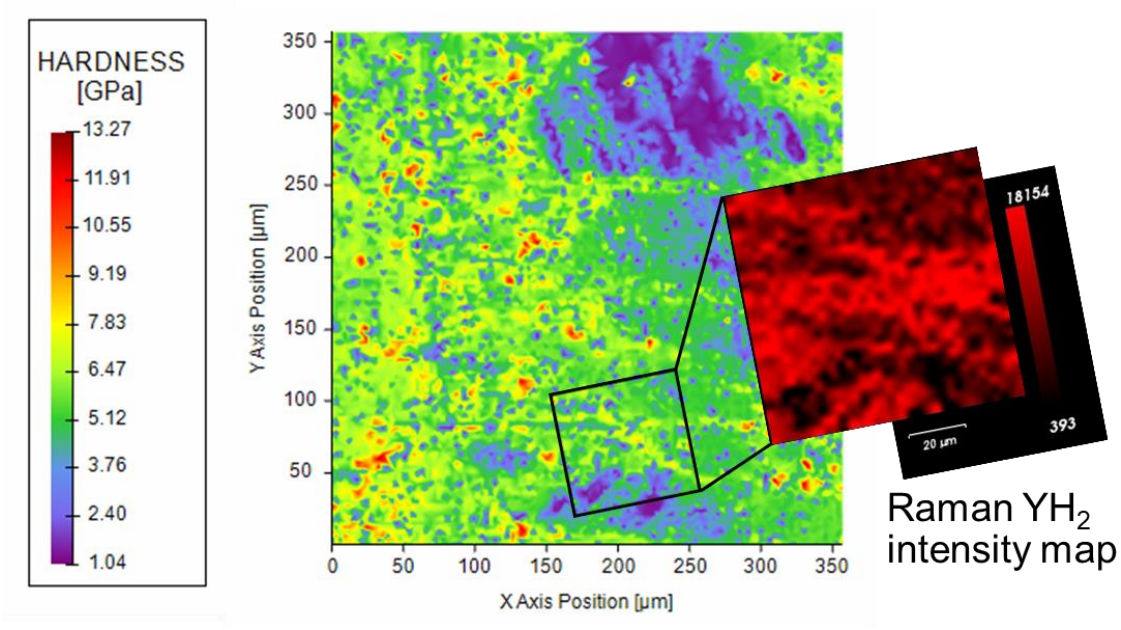

Figure 3. Nanoindentation hardness map of the $YH_{1.92}$ specimen. The Raman intensity map of the YH_2 peak based on integrated intensity from 1,055 to 1,225 cm^{-1} is inserted to compare the hardness distribution and Raman data.

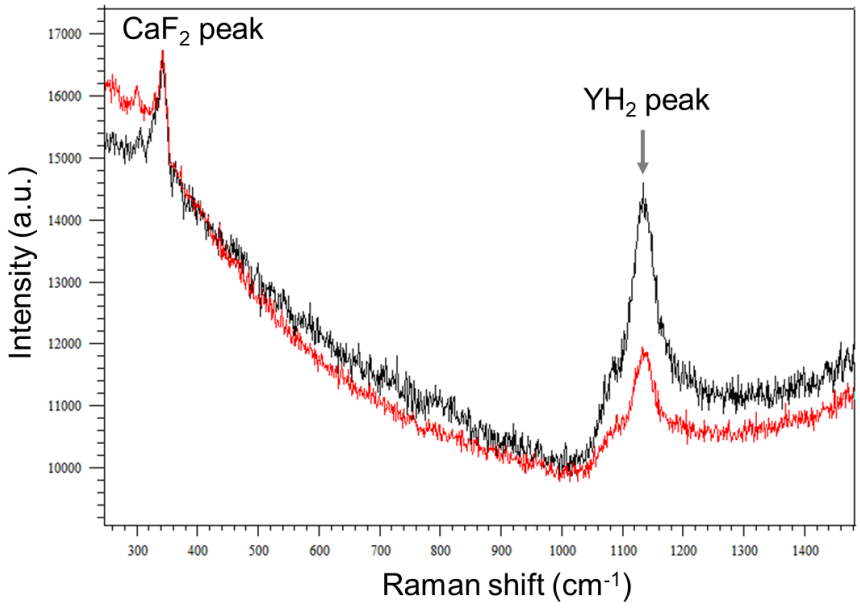

Figure 4. Raman spectra of the $YH_{1.92}$ specimen. The different intensity of the YH_2 peak obtained from the same specimen indicates nonuniform H distribution within the specimen.

The final experimental data presented are distributions of the nanoindentation modulus in the $YH_{1.00}$ and $YH_{1.92}$ specimen. A total of 14,400 indents was generated from a 360 × 360 µm area for each case. The indentation spacing was set to be 3 µm. The high-throughput mapping enables the statistical analysis of mechanical properties in the local areas. Figure 5 shows the bimodal distributions of the modulus in both $YH_{1.00}$ and $YH_{1.92}$ specimens. The black and red arrows in the graphs indicate the low and high peak moduli in the bimodal distributions, respectively. The high peak modulus represents the average modulus

of the yttrium hydride phase, whereas the low peak modulus is considered to be the modulus of the secondary phases (i.e., residual Y). The peak moduli of the hydride phase were 150–160 GPa for $YH_{1.00}$ and ~210 GPa for $YH_{1.92}$. This is reasonable because the higher H content results in a stiffer phase [2]. The peak of the $YH_{1.92}$ modulus was sharper than that of the $YH_{1.00}$ modulus, suggesting a more uniform H distribution in the $YH_{1.92}$ specimen. Both specimens had the lower modulus peak at ~30 GPa, implying a similar modulus of the secondary phase.

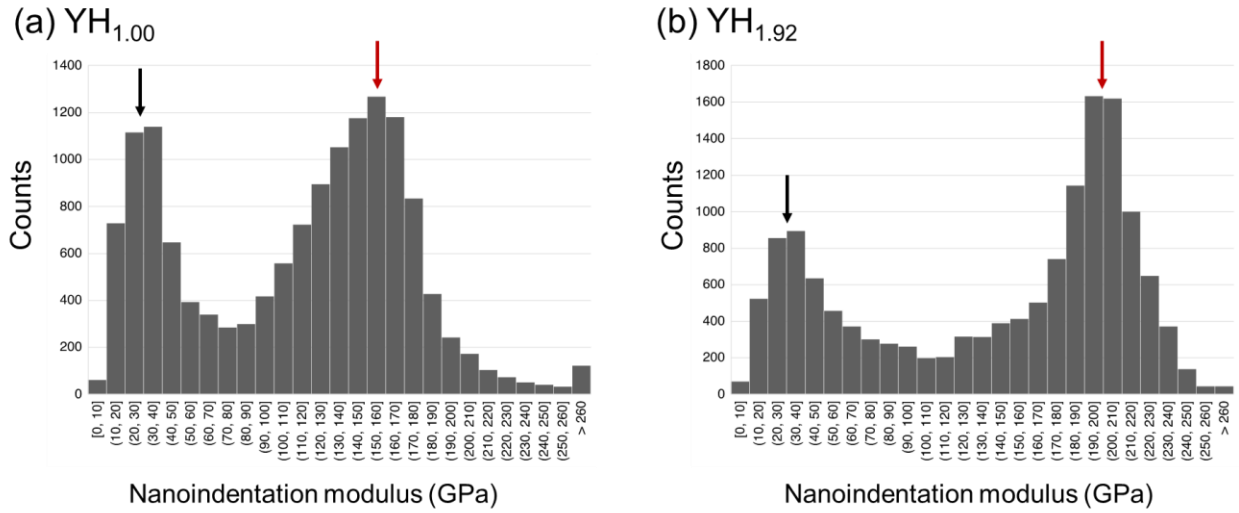

Figure 5. Distribution of nanoindentation modulus: (a) $YH_{1.00}$ and (b) $YH_{1.92}$ specimens. The black and red arrows indicate the low and high peak moduli in the bimodal distributions, respectively.

4. DISCUSSION

This study conducted semiquantitative mapping of H content in the yttrium hydrides through high-throughput nanoindentation mapping and Raman spectral imaging. Both methods use an indirect quantification approach. The nanoindentation hardness and modulus increase with increasing H content, which is expected from the bulk properties of yttrium hydrides [2]. The Raman intensity is expected to increase with increasing H content. The authors showed that the nanoindentation mapping and Raman imaging were complementary and that the experimental results from the two methods agreed with each other, as shown in Figure 3, although the results are preliminary. The methods proposed could be used to probe the local microstructure of hydrides in an area of up to 500 × 500 µm per map with a spatial resolution of a few micrometers or less. The map size is determined by the combination of practical maximum scan time and the spatial resolution. The spatial resolution of the nanoindentation mapping is approximately ten times the indentation depth [7] and is thus adjustable by changing the applied load. The spatial resolution of the Raman mapping typically ranges from 0.5–6 µm with a 532 nm laser, depending on the objective lens [12]. These spatial resolutions are far better than those of bulk testing methods proposed by Weiss [4]. Therefore, this study showed great progress in probing local hydride content at a microscopic scale, although neutron imaging could still be superior in terms of scan volume and accuracy [5]. The combination of the high-throughput nanoindentation mapping and Raman imaging could improve understanding of H desorption at different location and consequently help interpret the thermal desorption spectroscopy results.

Quantitative mapping is required to advance the nanoindentation and Raman mapping methods. This is enabled by using a set of reference hydride specimens with known H content and a uniform microstructure. The current available data are unsuitable for the reference because the bulk hardness and

elastic modulus reported by Hu and Terrani [2] are different from the nanoindentation hardness and modulus. Additionally, the relationship between the bulk properties and H/Y atomic ratio is apparent because of the presence of the residual Y and nonuniform H content within the specimens. Therefore, no experimental data are available for the intrinsic properties of yttrium hydride with different H/Y atomic ratios. Further study is required to process and characterize uniform yttrium hydride materials. Neutron scattering experiments are another option for bridging nanoindentation mechanical properties and stoichiometry.

To probe H content, a better understanding of the correlation among nanoindentation hardness and modulus, Raman spectra, and hydride microstructure is required. Crystallographic orientation could affect nanoindentation properties [13]. This study did not find any significant grain orientation dependence based on the comparison of the hardness map and EBSD result (Figure 2). Modeling nanoindentation behavior would improve understanding of the details of such effects as those studied for ZrH_2 [14]. Grain size is also an important factor for the nanoindentation mapping because grain and phase boundaries affect the results. In this study, the nanoindentation hardness and modulus were determined by the mechanical properties of the material volume within the deformation zone of the indent that is around 3 μm in diameter. Therefore, the intrinsic indentation hardness and modulus cannot be obtained if the grain size is relatively small compared with the deformation zone. The typical grain size (the equivalent circle diameter of the grain) was a few tens of micrometers in the $YH_{1.70}$ specimen based on the EBSD analysis (Figure 2b). This size might be large enough to measure the modulus and hardness from one grain. Similar considerations of the effects of microstructure are required to analyze Raman mapping. The Raman peak shape and intensity are affected by not only stoichiometry but also coherent domain size, which is affected by crystallinity, impurities, dislocations, and grain boundaries. This effect is significant for nano-sized crystals [15]. As such, future study requires the analysis of nanoindentation properties and Raman spectra by considering both stoichiometry (H/Y atomic ratio) and the microstructural feature for better probing the H content.

The findings of this study include the different nanoindentation modulus of yttrium hydride phases between the $YH_{1.00}$ and $YH_{1.92}$ specimens, as indicated by the statistical analysis; the moduli values are indicated by the red arrows in Figure 5. This is interesting because the YH_2 phase can have a very narrow composition of H concentration ranging from 65 to 66.6 at % at ambient temperature [8], but the modulus values between the two specimens were significantly different. The results imply an off-stoichiometric composition of yttrium hydride in a metastable state, which requires further investigation. The other finding is that there is nonuniform H distribution within the hydride specimens, as shown in Figure 2 and Figure 3. The results suggest that there is a room to improve the uniformity and purity of the hydride materials, although the specimens were fabricated after careful process optimization [6]. Such nonuniformity could affect the H desorption behavior because the inhomogeneous H distribution is a driving force of H thermal migration.

The proposed methods will also be useful for postirradiation examinations of yttrium hydrides. The size distribution of the secondary phase is expected to be a crucial microstructural parameter for the structural integrity of irradiated yttrium hydrides. One of the common degradation mechanisms of irradiated ceramics is irradiation-induced cracking due to swelling mismatch [16–18]. Therefore, microscopic-scale phase identification and characterization via the nanoindentation and Raman spectroscopy methods will provide insights of irradiation-induced cracking, if there are any. The proposed methods could also be used to investigate the thermo-migration and desorption of H after irradiation; nanoindentation hardness and/or modulus could probe local H content before and after irradiation based on the established correlation between the properties and stoichiometry. The statistical analysis (e.g., Figure 5) will be able to evaluate the elastic modulus of hydride phases that are not affected by residual Y. For the irradiation study, the data analysis must incorporate the effects of irradiation defects (e.g., point defects, dislocation loop, cavity) on the hardness and modulus in addition to the effects of stoichiometry. The modulus could

be more sensitive to stoichiometry change than irradiation defects, but hardness could also be highly affected by irradiation defects [19]. This requires further investigation. In summary, understanding local H content investigated by the proposed methods could be useful for performing a quality assessment of the yttrium hydride moderator.

5. SUMMARY AND NEXT STEPS

This study showed the potentials of the combination of the high-throughput nanoindentation mapping and Raman spectral imaging for probing local H content at a microscopic scale. Both methods use an indirect approach to determine the amount of H based on reference data of the relationship between the properties and stoichiometry. The nanoindentation mapping and Raman imaging are complementary, and comparing the results gives a better interpretation of the data. Additionally, phase identification via EBSD helped with data interpretation. This study conducted the semiquantitative analysis and revealed the nonuniform microstructure of the yttrium hydride specimens with three different H/Y atomic ratios.

The improved quantification will require reference specimens with a uniform microstructure and known H content to correlate the nanoindentation properties and Raman spectra to the stoichiometry of the hydride. Additionally, the interpretation of the nanoindentation and Raman results will require additional considerations of the effects of the microstructure (e.g., coherent grain size). The local material characterizations proposed in this study will be applied to yttrium hydride specimens before and after thermal desorption spectroscopy experiments to understand the H desorption of the specimens at both microscopic and macroscopic scales.

6. ACKNOWLEDGMENTS

This research was supported by the TCR program, which is supported by the US Department of Energy's (DOE's) Office of Nuclear Energy. The report was authored by UT-Battelle under contract no. DE-AC05-00OR22725 with the DOE.

The authors thank Xunxiang Hu at ORNL for preparing yttrium hydride specimens. Access to the Raman spectroscopy system was permitted by Andrew Miskowiec at ORNL. The authors also thank Tim Lach, Michael J. Lance, and Elizabeth Kirby at ORNL for the technical review and editing.

7. REFERENCES

[1] J.B. Vetrano, Hydrides as neutron moderator and reflector materials, Nucl. Eng. Des. 14 (1971) 390–412. doi:10.1016/0029-5493(70)90159-7.

[2] X. Hu, K.A. Terrani, Thermomechanical properties and microstructures of yttrium hydride, J. Alloys Compd. 867 (2021) 158992. doi:10.1016/j.jallcom.2021.158992.

[3] K.A. Terrani, B.C. Jolly, M.P. Trammell, G. Vasudevamurthy, D. Schappel, B. Ade, G.W. Helmreich, H. Wang, A.M. Rossy, B.R. Betzler, A.T. Nelson, Architecture and properties of TCR fuel form, J. Nucl. Mater. 547 (2021) 152781. doi:10.1016/j.jnucmat.2021.152781.

[4] Z. Weiss, Analysis of Hydrogen in Inorganic Materials and Coatings: A Critical Review, Hydrogen. 2 (2021) 225–245. doi:10.3390/hydrogen2020012.

[5] W. Gong, P. Trtik, A.W. Colldeweih, L.I. Duarte, M. Grosse, E. Lehmann, J. Bertsch, Hydrogen diffusion and precipitation in duplex zirconium nuclear fuel cladding quantified by high-resolution neutron imaging, J. Nucl. Mater. 526 (2019) 151757. doi:10.1016/j.jnucmat.2019.151757.

[6] X. Hu, D. Schappel, C.M. Silva, K.A. Terrani, Fabrication of yttrium hydride for high-temperature moderator application, J. Nucl. Mater. 539 (2020) 152335. doi:10.1016/j.jnucmat.2020.152335.

[7] P. Sudharshan Phani, W.C. Oliver, A critical assessment of the effect of indentation spacing on the measurement of hardness and modulus using instrumented indentation testing, Mater. Des. 164 (2019) 107563. doi:10.1016/j.matdes.2018.107563.

[8] D. Khatamian, F.D. Manchester, The H−Y (Hydrogen-Yttrium) system, Bull. Alloy Phase Diagrams. 9 (1988) 252–260. doi:10.1007/BF02881276.

[9] A.-M. Carsteanu, M. Rode, D. Zur, A. Borgschulte, H. Schröter, J. Schoenes, Short-range ordering in β− YH 2+ δ and β− YD 2+ δ thin films studied by Raman spectroscopy, Phys. Rev. B. 69 (2004) 134102. doi:10.1103/PhysRevB.69.134102.

[10] D. Olego, M. Cardona, Pressure dependence of Raman phonons of Ge and 3C-SiC, Phys. Rev. B. 25 (1982) 1151–1160. doi:10.1103/PhysRevB.25.1151.

[11] H. Richter, Z.P. Wang, L. Ley, The one phonon Raman spectrum in microcrystalline silicon, Solid State Commun. 39 (1981) 625–629. doi:10.1016/0038-1098(81)90337-9.

[12] A. Zoubir, ed., Raman Imaging, Springer Berlin Heidelberg, Berlin, Heidelberg, 2012. doi:10.1007/978-3-642-28252-2.

[13] Y. Liu, S. Varghese, J. Ma, M. Yoshino, H. Lu, R. Komanduri, Orientation effects in nanoindentation of single crystal copper, Int. J. Plast. 24 (2008) 1990–2015. doi:10.1016/j.ijplas.2008.02.009.

[14] L. Shi, M.L. Fullarton, S.R. Phillpot, Nanoindentation of ZrH2 by molecular dynamics simulation, J. Nucl. Mater. 540 (2020) 152391. doi:10.1016/j.jnucmat.2020.152391.

[15] A.K. Arora, M. Rajalakshmi, T.R. Ravindran, V. Sivasubramanian, Raman spectroscopy of optical phonon confinement in nanostructured materials, J. Raman Spectrosc. 38 (2007) 604–617. doi:10.1002/jrs.1684.

[16] T. Koyanagi, Y. Katoh, C. Ang, D. King, G.E. Hilmas, W.G. Fahrenholtz, Response of isotopically tailored titanium diboride to neutron irradiation, J. Am. Ceram. Soc. 102 (2019) 85–

89. doi:10.1111/jace.16036.
[17] C. Ang, C. Silva, C. Shih, T. Koyanagi, Y. Katoh, S.J. Zinkle, Anisotropic swelling and microcracking of neutron irradiated Ti3AlC2-Ti5Al2C3materials, Scr. Mater. 114 (2016) 74–78. doi:10.1016/j.scriptamat.2015.11.008.
[18] R.B. Matthews, Irradiation damage in reaction-bonded silicon carbide, J. Nucl. Mater. 51 (1974) 203–208. doi:10.1016/0022-3115(74)90003-8.
[19] N. Oono, R. Kasada, T. Higuchi, K. Sakamoto, M. Nakatsuka, A. Hasegawa, S. Kondo, N.Y. Iwata, H. Matsui, A. Kimura, Comparison of irradiation hardening and microstructure evolution in ion-irradiated delta and epsilon hydrides, J. Nucl. Mater. 442 (2013) S826–S829. doi:10.1016/j.jnucmat.2013.03.013.